IOP Publishing Smart Materials and Structures
Smart Mater. Struct. **16** (2007) R23–R31 doi:10.1088/0964-1726/16/6/R01

TOPICAL REVIEW

Review of modeling electrostatically actuated microelectromechanical systems

R C Batra[1], **M Porfiri**[2] **and D Spinello**[1]

[1] Department of Engineering Science and Mechanics, Virginia Polytechnic Institute and State University, Blacksburg, VA 24061, USA
[2] Department of Mechanical, Aerospace and Manufacturing Engineering, Polytechnic University, Brooklyn, NY 11201, USA

E-mail: rbatra@vt.edu, mporfiri@poly.edu and dspinell@vt.edu

Received 10 February 2007, in final form 23 August 2007
Published 8 October 2007
Online at stacks.iop.org/SMS/16/R23

Abstract
A wide range of microelectromechanical systems (MEMSs) and devices are actuated using electrostatic forces. Multiphysics modeling is required, since coupling among different fields such as solid and fluid mechanics, thermomechanics and electromagnetism is involved. This work presents an overview of models for electrostatically actuated MEMSs. Three-dimensional nonlinear formulations for the coupled electromechanical fluid–structure interaction problem are outlined. Simplified reduced-order models are illustrated along with assumptions that define their range of applicability. Theoretical, numerical and experimental works are classified according to the mechanical model used in the analysis.

1. Introduction

Recent technological developments have opened up promising research opportunities and engineering priorities in micromechanics. It is now possible to manufacture mechanical parts such as resonators, sensors, gears, and levers on a micron lengthscale, and to produce tiny needles to inject fluid into a living organism without stimulating nerve cells. The use of existing integrated circuit technology in the design and production of microelectromechanical systems (MEMSs) allows these devices to be batch-manufactured, thereby reducing the production cost. The thorough understanding, prediction, and control of MEMSs behavior at the microscale are critical issues. Multiphysics modeling is required, since coupling among different fields such as solid and fluid mechanics, thermomechanics and electromagnetism is involved.

MEMSs find wide applications as sensors and actuators. The analysis of methods of actuation and sensing has been a topic of interest over the past several years. Different actuation and sensing properties such as piezoresistive, piezoelectric, electrostatic, thermal, electromagnetic, and optical have been used. Comparisons among MEMSs based on these properties, and of fabrication methods, can be found in [1–3]. There is no one optimal sensing and actuating method, and the choice mainly depends on the particular application.

Electrostatics is often the preferred sensing and actuating technique [1]. An electrostatically actuated MEMS is generally an elastic perfect conductor suspended above a stationary rigid perfect conductor (see e.g. [4]) with a flat top surface. A dielectric medium, usually air, fills the gap between them. The overall system behaves as a variable gap capacitor. An applied DC voltage is used to induce displacements of the deformable body, and a consequent change in the system capacitance. Typical applications are transistors, switches, micro-mirrors, pressure sensors, micro-pumps, moving valves and micro-grippers; see e.g. [5–11]. When an AC component is superimposed on the steady voltage to excite harmonic motions of the system, resonators are obtained. These devices are used in signal filtering, and chemical and mass sensing; see e.g. [12–19].

The applied electrostatic voltage has an upper limit beyond which electrostatic force is not balanced by the elastic restoring force in the deformable conductor that eventually snaps and touches the lower rigid plate, and the MEMS collapses. This phenomenon, called pull-in instability, has been observed experimentally [20, 21]. The critical

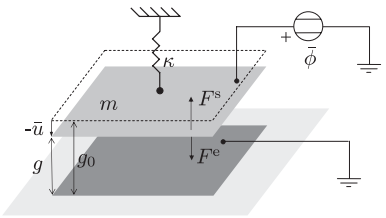

Figure 1. Sketch of the lumped spring–mass system.

displacement, and the critical voltage associated with this instability, are called pull-in displacement and pull-in voltage, respectively. Their accurate evaluation is crucial in the design of electrostatically actuated MEMSs. In particular, in micro-mirrors [8] and micro-resonators [22] the designer avoids this instability in order to achieve stable motions; however, in switching applications [6] the designer exploits this effect to optimize the performance of the device.

A simple lumped spring–mass system for estimating pull-in parameters is proposed in [21] (see figure 1). The elasticity of the deformable body is lumped into the spring stiffness κ, F^s is the spring restoring force, $\bar{\phi}$ is the applied voltage, F^e is the electrostatic force, m is the mass of the movable electrode, g_0 is the initial gap between the two conductors, $\bar{u}$ is the displacement of the movable electrode, A is the electrode's area, ϵ is the dielectric constant of the dielectric medium between the two electrodes, and $g = g_0 + \bar{u}$ is the actual gap. F^e exceeds F^s near the pull-in unstable condition, and the pull-in parameters are

$$\bar{\phi}_{\mathrm{PI}} = \sqrt{\frac{8\kappa g_0^3}{27\epsilon A}}, \qquad g_{\mathrm{PI}} = \frac{2}{3} g_0.$$

The pull-in voltage $\bar{\phi}_{\mathrm{PI}}$ so obtained usually exceeds that observed experimentally for many applications [23]. Moreover, the lumped spring–mass model does not incorporate inherent nonlinearities of the electrostatic and the restoring forces [11, 24], resulting in poor estimates of the pull-in gap g_{PI} and the pull-in voltage $\bar{\phi}_{\mathrm{PI}}$.

The rest of the paper is organized as follows. In section 2 we formulate the three-dimensional (3D) nonlinear problem and cite available studies. In section 3, simplified distributed models are illustrated, along with numerical and experimental results. Section 4 gives a brief survey of additional effects appearing at the nanoscale in the miniaturization of MEMSs. Section 5 gives a summary of works in a table.

2. Three-dimensional problem

2.1. Coupling in MEMSs

The following example to illustrate the coupling phenomenon in MEMSs is taken from [25]. Consider the electrostatically actuated cantilever microbeam shown in figure 2. Air fills the gap between the two conductors and the medium surrounding the device. When a potential difference $\bar{\phi}$ is applied between the top deformable electrode and the bottom immovable plate, electrostatic charges are induced on surfaces of the conductors (figure 2(a)). These charges generate an electrostatic pressure (see section 2.4). As a consequence, the movable electrode deforms against the viscous fluidic force (see section 2.5), the charges redistribute on surfaces of the conductors, and the electrostatic force changes (figure 2(b)) till the system reaches an equilibrium configuration.

2.2. Problem statement and geometry

We model the deformable conductor as a solid elastic body undergoing finite deformations. The deformable and the fixed rigid body are considered as perfect conductors. From an electric point of view air is modeled as a homogeneous isotropic dielectric, while, from a mechanical point of view, it is regarded as a compressible Newtonian fluid. We assume that the temperature does not change during the motion. Deformations of movable conductors are stated in the Lagrangian description, while air motion and electrostatic field are stated in the Eulerian description, see e.g. [26].

The notation is illustrated in figure 2. We denote the reference configuration of the deformable conductor by Ω. A point $\mathbf{p} \in \Omega$ is called a material point. The motion is indicated by x, and the reference map by p. The present configuration at time t is $\Omega_t = \mathsf{x}(\Omega, t)$, and points in the present configuration are $\mathbf{x} = \mathsf{x}(\mathbf{p}, t)$. The outward normal to $\partial\Omega$ at $\mathbf{p}$ is denoted by $\mathbf{n}(\mathbf{p})$, and the outward normal to $\partial\Omega_t$ at $\mathbf{x}$ by $\mathbf{m}(\mathbf{x})$. The part of the boundary $\partial\Omega$ where essential boundary conditions are prescribed is $\Gamma_{\mathbf{u}}$. The part of $\partial\Omega$ where natural boundary conditions are assigned is $\Gamma_{\mathbf{t}}$. The configuration of the immovable conductor is Ω_0. At time t air occupies an unbounded portion of the ambient space $\mathcal{E}$, defined by $\bar{\Omega}_t = \mathcal{E} - \Omega_t$. Points in $\bar{\Omega}_t$ are identified by $\mathbf{x}$, as is done for points of the present configuration of the deformable electrode. For a planar deformable conductor (e.g. a plate) we identify the point $\mathbf{x}$ with the pair $(\hat{\mathbf{x}}, z)$, where $\hat{\mathbf{x}}$ is the projection of $\mathbf{x}$ on the fixed conductor plane, and $z = \mathbf{x}\cdot\mathbf{e}$ is the component along the normal $\mathbf{e}$ of the fixed conductor plane. A point located

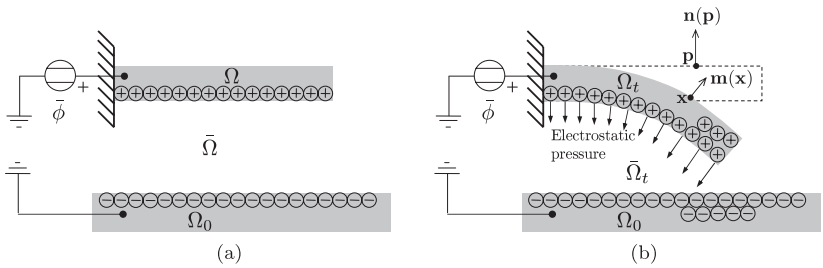

Figure 2. Simple example to illustrate electromechanical coupling in electrostatic MEMSs.

on the movable planar conductor boundary closer to the fixed conductor is characterized by $(\hat{\mathbf{x}}, g)$.

The material description of a spatial field $(\cdot)$ is denoted by $(\cdot)_{\mathrm{m}}$. Spatial gradient and divergence are indicated by grad and div respectively. Material or referential gradient and divergence are denoted by Grad and Div. A superimposed dot means material time derivative.

2.3. Mechanical deformations

An electrostatically actuated MEMS can undergo large deformations depending on its geometry and applied voltage. Here we outline governing equations for large deformations of a MEMS wherein the deformable electrode is modeled as a 3D continuum.

The equilibrium equations in the Lagrangian description of motion are [26]

$$\varrho_0 \ddot{\mathbf{u}} = \mathrm{Div}\mathbf{F}\mathbf{S}, \tag{1a}$$

$$\mathbf{S} = \mathbf{S}^{\mathrm{T}}. \tag{1b}$$

Equations (1*a*) and (1*b*) are the balance of linear momentum, and the balance of moment of momentum respectively. $\mathbf{S}$ is the second Piola–Kirchhoff stress tensor, $\mathbf{u} = \mathbf{x} - \mathbf{p}$ the displacement field, $\mathbf{F} = \mathbf{1} + \mathrm{Grad}\mathbf{u}$ the deformation gradient, $\mathbf{1}$ the second-order identity tensor, ϱ_0 the mass density in the reference configuration, and T means transposition.

For an elastic material, the constitutive equation for $\mathbf{S}$ is [26]

$$\mathbf{S} = \hat{\mathbf{S}}(\mathbf{F}) \tag{2}$$

where $\hat{\mathbf{S}}$ represents the response function for the material. Equations (1*a*), (1*b*) and (2) are supplemented with the following boundary conditions:

$$\mathbf{u} = \bar{\mathbf{u}} \qquad \text{on } \Gamma_{\mathbf{u}}, \qquad \mathbf{P}\mathbf{n} = \bar{\mathbf{t}} \qquad \text{on } \Gamma_{\mathbf{t}}, \tag{3}$$

and initial conditions

$$\mathbf{u}(\mathbf{p}, 0) = \mathbf{u}_0(\mathbf{p}), \qquad \dot{\mathbf{u}}(\mathbf{p}, 0) = \mathbf{v}_0(\mathbf{p}), \tag{4}$$

where $\mathbf{P} = \mathbf{F}\mathbf{S}$ is the first Piola–Kirchhoff stress tensor, and $\bar{\mathbf{t}}$ is the surface traction per unit undeformed area. Furthermore, $\mathbf{u}_0$ and $\mathbf{v}_0$ give, respectively, the initial displacement and the initial velocity fields.

The traction exerted at the point $\mathbf{x}$ of the boundary $\partial\Omega_t$ is comprised of the electrostatic traction $f^{\mathrm{e}}(\mathbf{x})\mathbf{m}(\mathbf{x})$ and of the traction $\mathbf{t}^{\mathrm{a}}(\mathbf{x})$ exerted by air. We note that the electrostatic traction acts along the normal to the boundary as a consequence of the assumption that the body is a perfect conductor. We refer to f^{e} as the electrostatic pressure. On the other hand, the fluidic traction does not, in general, act along the normal due to air viscosity. The traction exerted by air equals $\mathbf{T}\mathbf{m}$, where $\mathbf{T}$ is the fluid Cauchy stress tensor. The traction in the reference configuration at point $\mathbf{p}$ and time t is given by

$$\bar{\mathbf{t}}(\mathbf{p}, t) = \left[(\det\mathbf{F})(f^{\mathrm{e}}\mathbf{1} + \mathbf{T})\mathbf{F}^{-\mathrm{T}}\mathbf{n}\right](\mathbf{p}, t). \tag{5}$$

In order to solve the initial-boundary-value problem defined by equations (1*a*), (1*b*), (2), (3) and (4), we need an explicit form of the material response function $\hat{\mathbf{S}}$ in (2), and of the electrostatic pressure f^{e} and the fluid Cauchy stress tensor $\mathbf{T}$ in (5). The response function $\hat{\mathbf{S}}$ depends on the deformable electrode's material, while the electrostatic and fluidic tractions are coupled to the electrostatic and fluid problems described below. Similar multiphysics problems are encountered in aeroelasticity [27].

2.4. Electrostatic force

Because of the very high speed of electric waves as compared to that of the mechanical waves, we presume that inertia effects in the electric field are negligible. The boundary-value problem for the electrostatic potential ϕ formulated in the present configuration is (see e.g. [28])

$$\mathrm{div}\,\mathrm{grad}\,\phi = 0 \qquad \text{in } \bar{\Omega}_t, \tag{6a}$$

$$\phi = \bar{\phi} \qquad \text{on } \partial\Omega_t, \tag{6b}$$

$$\phi = 0 \qquad \text{on } \partial\Omega_0, \tag{6c}$$

$$\phi \to 0 \qquad \text{as } \|\mathbf{x}\| \to \infty. \tag{6d}$$

The electrostatic potential energy U^{e} stored in $\bar{\Omega}_t$ for the two-conductor system is given by

$$U^{\mathrm{e}} = \frac{\epsilon}{2}\int_{\bar{\Omega}_t} \mathrm{grad}\phi \cdot \mathrm{grad}\phi \,\mathrm{d}\bar{\Omega}_t, \tag{7}$$

where ϵ is the dielectric constant of air. The electrostatic pressure at the point $\mathbf{x}$ in the present configuration is given by

$$f^{\mathrm{e}}(\mathbf{x}) = -\frac{\epsilon}{2}\left[\mathrm{grad}\phi \cdot \mathrm{grad}\phi\right](\mathbf{x}). \tag{8}$$

Using the relation

$$\mathrm{Grad}\phi_{\mathrm{m}} = \mathbf{F}^{\mathrm{T}}\mathrm{grad}\phi,$$

for the material description of the electrostatic pressure at the observation point $\mathbf{p}$ in the reference configuration, we get

$$f^{\mathrm{e}}_{\mathrm{m}}(\mathbf{p}) = -\frac{\epsilon}{2}\left[\mathrm{Grad}\phi_{\mathrm{m}} \cdot \left(\mathbf{F}^{\mathrm{T}}\mathbf{F}\right)^{-1}\mathrm{Grad}\phi_{\mathrm{m}}\right](\mathbf{p}). \tag{9}$$

Using potential theory, the solution of the boundary-value problem (6*a*)–(6*d*) can be written as a boundary integral [29]:

$$\phi(\mathbf{x}) = \int_{\partial\Omega_t \cup \partial\Omega_0} G(\mathbf{x}, \mathbf{y})\sigma(\mathbf{y})\,\mathrm{d}\gamma_t(\mathbf{y}) + c_{\mathrm{T}}, \tag{10}$$

where $\mathbf{x}$ and $\mathbf{y}$ are the observation and the source points on $\partial\Omega_t \cup \partial\Omega_0$, σ is the surface charge density, G the Green function, and $\mathrm{d}\gamma_t$ the area element. The constant c_{T} is determined from the potential at infinity. Equation (10) gives the electrostatic potential in the present configuration of the system. The area element $\mathrm{d}\gamma_t$ is expressed in terms of the corresponding area element $\mathrm{d}\gamma$ by (see [26])

$$\mathrm{d}\gamma_t^2 = (\det\mathbf{F})^2(\mathbf{n} \cdot (\mathbf{F}^{\mathrm{T}}\mathbf{F})^{-1}\mathbf{n})\,\mathrm{d}\gamma^2. \tag{11}$$

Therefore, equation (10) can be written in the Lagrangian description of motion as

$$\phi_{\mathrm{m}}(\mathbf{p}) = \int_{\partial\Omega\cup\partial\Omega_0} G_{\mathrm{m}}(\mathbf{p}, \mathrm{p}(\mathbf{y}))\sigma_{\mathrm{m}}(\mathrm{p}(\mathbf{y}))(\det\mathbf{F}) \times \sqrt{\mathbf{n} \cdot \left(\mathbf{F}^{\mathrm{T}}\mathbf{F}\right)^{-1}\mathbf{n}}\,\mathrm{d}\gamma(\mathbf{y}) + c_{\mathrm{T}}. \tag{12}$$

2.5. Viscous damping

The equilibrium equations in the Eulerian description of motion for the air are [26]

$$\dot{\rho} + \rho \mathrm{div}\mathbf{v} = 0, \tag{13a}$$

$$\rho\dot{\mathbf{v}} = \mathrm{div}\mathbf{T}, \tag{13b}$$

$$\mathbf{T} = \mathbf{T}^{\mathrm{T}}. \tag{13c}$$

Equations (13*a*), (13*b*) and (13*c*) are the balance of mass, the balance of linear momentum and the balance of moment of momentum, respectively. $\mathbf{T}$ is the fluid Cauchy stress tensor, $\mathbf{v}$ the fluid velocity field, ρ the fluid mass density in the present configuration, and a superimposed dot indicates the material time derivative.

For a compressible Newtonian ideal gas, the constitutive equations for $\mathbf{T}$ and the fluid pressure π are [30]

$$\mathbf{T} = -\left(\pi + \tfrac{2}{3}\mu \mathrm{div}\mathbf{v}\right)\mathbf{1} + 2\mu\mathbf{D}, \tag{14}$$

$$\pi = \rho RT, \tag{15}$$

where μ is the shear viscosity, $\mathbf{D} = \mathrm{Symgrad}\mathbf{v}$ the fluid stretching or the strain-rate tensor, R the ideal gas constant, T the absolute temperature, and we have employed Stoke's approximation [30]. Symgrad$\mathbf{v}$ equals the symmetric part of grad$\mathbf{v}$. By substituting (14) into (13*b*) one obtains the Navier–Stokes equation:

$$\rho\dot{\mathbf{v}} = -\mathrm{grad}\left(\pi - \frac{\mu}{3}\mathrm{div}\mathbf{v}\right) + \mathrm{div}(\mu\,\mathrm{grad}\mathbf{v}). \tag{16}$$

Equations (16), (13*a*) and (15) are completed with the following boundary conditions:

$$\mathbf{v}(\mathbf{x}, t) = \dot{\mathsf{x}}(\mathsf{p}(\mathbf{x}, t), t) \qquad \text{on } \partial\Omega_t, \tag{17}$$

$$\mathbf{v} = \mathbf{0} \qquad \text{on } \partial\Omega_0, \tag{18}$$

$$\mathbf{v} \to \mathbf{0} \qquad \text{as } \|\mathbf{x}\| \to \infty, \tag{19}$$

and initial conditions

$$\mathbf{v}(\mathbf{x}, 0) = \mathbf{0}, \qquad \rho(\mathbf{x}, 0) = \rho_0(\mathbf{x}), \tag{20}$$

where we assumed that the fluid is initially at rest. Boundary conditions (17) and (18) state that the relative velocity between the electrodes and the fluid is zero.

2.6. References for results

Numerous computer algorithms based on the finite-element (FE) formulation of the above-stated 3D problem have been developed [31–34] and used to simulate MEMSs [35, 23]. In [36] a meshless numerical formulation has been proposed to analyze MEMSs. In [37, 38] a potential theory formulation in the Lagrangian description of motion (equation (12)) of the electrostatic problem for two-conductor systems comprised of deformable bodies has been numerically solved. The Lagrangian description of motion has been used in [25, 39] to numerically solve the MEMS multiphysics problem with coupling between the electrostatic and the mechanical fields; in [40] the coupling of hierarchical fluid models with the electromechanical domain has also been included. In [41] there is presented an algorithm for extracting the pull-in parameters of electrostatic actuators based on iterating the displacement of a pre-chosen degree-of-freedom of a node of the actuator. Different computational techniques to optimize the 3D algorithms are reported in [42].

Results of numerical simulations can be found in [43, 23, 44]. In [43], corrections to ideal models of fixed–fixed microbeams due to fringing fields, the assumption of plane-strain deformations and anchor compliance are studied, while in [44] pull-in parameters of micromachined cantilevers are extracted including the effects of residual stresses and somewhat realistic boundary conditions. In [23], effects of partially electroded conductors, of axial stress, nonlinear stiffening, charge redistribution and fringing fields are included in the simplified lumped mass–spring models of fixed–fixed and cantilever microbeams.

3. Reduced-order models

In order to alleviate the computational expense associated with the 3D analysis, considerable efforts have been devoted to the development of reduced-order distributed models for MEMSs. Approximations can be made in any one of the three domains of the multiphysics MEMS analysis: mechanical, electrical and fluidic.

The deformable electrode can be modeled as a beam or as a plate depending upon its geometry. Theories of beams (1D) and plates (2D) can be derived intrinsically (see e.g. [45, 46]), or can be deduced from the full 3D theory (see e.g. [45, 47–50]). Beam theory is generally applicable to slender bodies whose cross-sectional dimensions are significantly smaller than their lengths [51]. Plate theory is applicable to a flat body whose thickness is significantly smaller than the width and the length [51]. Beam theory is also applicable to plate-like bodies undergoing cylindrical bending deformations; in this case the body is usually referred to as a wide beam. String and membrane theories can be viewed as further simplifications of beam and plate theories, respectively, that are suitable when the body rigidity due to in-plane stretching dominates over the bending stiffness [52]. This generally is valid for extremely thin prestressed bodies.

For relatively small gaps between the two conductors with respect to the in-plane dimensions of the deformable conductor, the two conductors can be considered to be locally parallel to each other. The electrostatic pressure can be expressed using the parallel-plate approximation [4, 28] as

$$f^{\mathrm{e}}(\mathbf{x}) = -\frac{\epsilon\bar{\phi}^2}{2g(\hat{\mathbf{x}})^2}, \tag{21}$$

where $\mathbf{x} = \hat{\mathbf{x}} + g(\hat{\mathbf{x}})\mathbf{e}$ is a point on the movable conductor separated by a gap $g(\hat{\mathbf{x}})$ from the fixed conductor. In this approximation, fringing fields emanating from the top and the lateral surfaces of the movable conductor are discarded. For narrow geometries, fringing fields can be taken into account by correcting the parallel-plate approximation using Palmer's formula [53], the Mejis–Fokkema formula [54], or those given in [55, 56]. Estimates of the electrostatic pressure based on the parallel-plate approximation are not influenced by spatial derivatives of the function g and are suitable only when

$g_0/L \ll 1$, where L is the length of the deformable conductor. For larger gaps, more accurate estimates can be developed by considering the slope and the curvature of the deformable electrode [57, 58].

The Navier–Stokes equation (16) can be considerably simplified under the hypotheses of $g_0/L \ll 1$, slow motions with the dominant motion in the gap direction [1]. In this case the inertia term on the left-hand side of equation (16) can be discarded, and on the right-hand side the terms involving derivatives of the in-plane velocity with respect to the gap direction and velocity component along the gap direction can be neglected. As a result the fluidic pressure π can be determined through the Reynolds equation of lubrication [59]:

$$12\mu\frac{\partial(\pi g)}{\partial t}(\hat{\mathbf{x}},t) + \hat{\mathrm{div}}(g^3\pi\hat{\mathrm{grad}}\pi)(\hat{\mathbf{x}},t) = 0, \qquad (22)$$

where $\hat{\mathrm{div}}$ and $\hat{\mathrm{grad}}$ are the divergence and the gradient operators with respect to in-plane coordinates. Because of the assumption that the distance g_0 between the two electrodes is much smaller than the characteristic length L, the pressure is uniform in the gap direction z, i.e. $\partial\pi/\partial z = 0$ [59]. For relatively large gaps, a solution of the full Navier–Stokes equations is required to find accurate estimate of the air damping [40]. In order to account for rarefication effects, the viscosity may be replaced by an effective viscosity depending on the Knudsen number [1, 60]. Different boundary conditions for the Reynolds equation have been studied to improve the accuracy of the approximation [61]. Problems for perforated conductors have also been studied [62].

We summarize below prior studies classified according to the mechanical model used in the analysis. The description of mathematical models has been omitted because of a limitation on the number of pages.

3.1. Beams

In [12, 63–65, 15, 66, 67] the pull-in instabilities of wide rectangular microbeams in vacuum are studied. In [15], the linear Euler–Bernoulli beam theory in conjunction with the parallel-plate approximation is used. The Euler–Bernoulli beam theory is valid for thin beams undergoing small deformations. Pull-in instability is determined using the Rayleigh–Ritz method. In [65], the linear Euler–Bernoulli beam theory is also used, but the parallel-plate approximation is corrected using Palmer's formula that accounts for fringing fields emanating from the beam top-surface. The finite-difference method is used to determine pull-in parameters and approximate empirical formulas are provided. In [66], the string theory and the plate approximations are used, and closed-form expressions for pull-in parameters are derived. In [12, 67], the deformable conductor is modeled as a von-Karman plate undergoing cylindrical deformations, and the parallel-plate approximation is used to find the electrostatic pressure. The von-Karman plate theory results in a nonlinear governing equation since it accounts for mid-plane stretching and allows for studying moderately large displacements. The importance of mid-plane stretching on microbeam's deformations was pointed out in [68]. In [12], the pull-in instability is studied using the shooting method. In [67], reduced-order models and perturbation techniques are utilized to analyze the pull-in behavior. An overview of reduced-order modeling techniques for MEMSs can be found in [69]. In [63], plane deformations of the movable electrode are modeled using a nonlinear beam theory, and the electrostatic pressure is determined by solving with the finite-element method (FEM) the full 2D electrostatic problem. In [64], a linear beam theory is used to describe the motion of the deformable electrode, and the electrostatic pressure is found by solving the 3D electrostatic problem with the finite-difference method.

The static behavior of wide microbeams in vacuum after pull-in instability is studied in [70]. The device is modeled as in [15] and the finite-difference method is used to analyze the problem.

Transient and forced oscillations in vacuum of wide rectangular beams are presented in [16, 71–75]. In [16, 71, 73], the modeling framework of [12] and reduced-order models [67] are used. In [16] perturbation techniques are employed to study primary resonances. In [71] and [73], secondary resonances are explored; perturbation techniques are utilized in [71], while a thorough nonlinear analysis is performed in [73]. In [74], a nonlinear beam theory is used to describe large deformations of the deformable electrode and the electrostatic pressure is computed by solving the full 2D electrostatic problem using the FEM. In [76], alternative configurations of the movable and fixed electrodes are examined using reduced-order models and the framework of [12]. In [72], the model of [65] is analyzed using a numerical method based on the radial basis functions.

In [18], the model of [12] is extended to microbeams with variable cross sections, and the pull-in instability is analyzed by studying small vibrations in vacuum. In [77], the findings of [18] are generalized to forced and transient nonlinear oscillations. In [77], the parallel-plate approximation is used, while in [18] the Palmer formula is adopted. In both [18] and [77] the differential quadrature method is used to find an approximate solution of the nonlinear governing equations.

In [78], the effects of fringing fields on the pull-in parameters of narrow rectangular beams in vacuum are analyzed. The parallel-plate approximation is improved by considering fringing fields emanating from the lateral and the top surfaces of the deformable electrode that is modeled using the von-Karman plate theory. The pull-in parameters are extracted by using both the meshless local Petrov–Galerkin method [79–81] and the Rayleigh approximation based on a one-degree-of-freedom system. In [82], the model of [78] is used to analyze small vibrations. The resonance frequencies, in general, do not monotonically decrease with an increase in the voltage applied between the two conductors [12, 82].

In [83–86], a dynamic analysis of wide microbeams incorporating the combined effects of the electrostatic pressure and the fluidic traction is performed. In [84, 86], the microbeam is modeled with the linear beam theory, the parallel-plate approximation is used for the electrostatic pressure, and the lubrication theory for the air pressure. In [84], a neuro-network-based method for model reduction is proposed to rapidly analyze the system transient response, while in [86] the Galerkin method is used to study small vibrations. In [83, 85], rarefication effects due to low pressure are also considered, and the transient response is studied using reduced-order models. In [85], thermal effects on the transient response are also studied.

Table 1. Summary of the electromechanical models presented in the paper. Abbreviations FE, BE, FD, DQ and ROM are used for finite element, boundary element, finite difference, differential quadrature, and reduced-order-model, respectively.

		Mechanical model					
		3D analysis	von Karman plate	Kirchhoff plate	Linear membrane	Nonlinear beam	Linear beam
Electrostatic force	Parallel plate		[93, 94]	[90, 91]	[95, 96]	[12, 67, 16, 71]	[15, 70, 84]
	— (cntd)			[92, 60]	[28, 97]	[73, 76, 77]	[86, 83, 85]
	Fringing fields					[18, 78, 82, 23]	[65, 72, 43]
	3D analysis	[25, 39]	[87–89]			[63, 74]	[64]
Viscous damping	Squeeze film			[60]			[84, 86, 83, 85]
	3D analysis	[40]					
Solution technique	FE/BE/FD	[32, 34, 35, 23]	[87–89]			[63, 74, 78]	[65, 64, 70]
	Meshless	[25, 39, 40]			[97]	[78]	[72]
	ROM		[93, 94]	[60]	[83, 85]	[67, 16, 71, 73]	[15]
	— (cntd)					[76, 78, 82, 23]	
	Shooting/DQ				[95, 96, 28]	[12, 18, 77]	

3.2. Plates

Static deformations of microplates in vacuum are studied in [87, 88]. The von-Karman plate theory is adopted to model large deflections of the microplate, and the boundary-element method is used to solve the electrostatic problem and compute the electrostatic pressure. The same modeling framework is used in [89] to analyze transient deformations of microplates in vacuum.

In [90–92], microplates in vacuum are studied using a linear plate theory and the parallel-plate approximation. In [90], closed-form expressions for pull-in parameters are established using a reduced-order model. In [91], thermoelastic damping is considered and numerical estimates of quality factors are established using perturbation techniques. In [92], a different configuration of electrodes with the actuation voltage applied across a confined fluid is studied using reduced-order models.

The pull-in instability and small vibrations of microplates in vacuum are studied in [93, 94]. The von-Karman plate theory is used to model large deflections of the deformable plate and the parallel-plate approximation is used for the electrostatic pressure. Rectangular geometries are considered in [93], and circular in [94]. Numerical analysis is performed with reduced-order models.

Pull-in instabilities of thin microplates using a linear membrane theory and the parallel-plate approximation are considered in [95, 96, 28, 97]. Due to symmetry in the distributed electrostatic load and boundary conditions, simple 1D models of rectangular and circular micromembranes have been adopted in [95, 96]. In [97], the governing partial differential equations for 2D deformations have been solved by implementing the pseudoarclength algorithm [98] in a meshless method. In [28] the idealized MEMS is embedded in a control circuit to analyze various schemes for controlling the pull-in instability.

Small vibrations of microplates in air are studied in [60]. A linear plate theory is used to model the deformable electrode, the parallel-plate approximation is adopted to compute the electrostatic pressure, and the lubrication theory for rarefied gases is employed to model the air dynamics. The analysis is conducted through a combination of perturbation techniques and the FEM.

4. Miniaturization of MEMSs: additional effects at the nanoscale

With the decrease in device dimensions from the microscale to the nanoscale, additional forces on nanoelectromechanical systems (NEMSs), such as the Casimir force [99, 100], should be considered. The Casimir force constrains the miniaturization of electrostatically actuated devices. At the nanoscale, the Casimir force may overcome elastic restoring actions in the device and lead to the bodies' sticking during the fabrication process.

For semi-infinite parallel-plate-like conductors, the attractive Casimir traction between them is given by [101]

$$f^{c}(\mathbf{x}) = -\frac{\hbar c \pi^2}{240 g(\hat{\mathbf{x}})^4}, \tag{23}$$

where $\hbar$ is Plank's constant and c the speed of light in vacuum. Theoretical works devoted to estimating corrections to the Casimir pressure given by equation (23) for geometries with known and fixed departures from the parallel configuration can be found in [102, 103]. However, equation (23) is consistent with the assumptions introduced in the mechanical and the electrostatic models when the small deformations plate theory or a linear beam theory together with the parallel-plate approximation is adopted.

Theoretical and experimental analysis of the stiction phenomenon in NEMSs can be found in [104–108]. The effect of the Casimir force on the pull-in parameters of NEM switches is investigated in [109] through a reduced one-degree-of-freedom model. In [110], the combined effect of the electrostatic and the Casimir forces on rectangular membrane strips is studied with a distributed 1D model, while in [111], a 2D distributed model is used to study different geometries. von Karman microplates under the combined effect of the Coulomb and the Casimir forces are studied in [112, 113].

The van der Waals forces, related to the electrostatic interaction among dipoles at the atomic scale [114], depend on material properties of the media, and are effective at shorter distance than the Casimir force, when the separation is less than the retardation length which corresponds to the transition between the ground and the excited states of the atom [114].

The van der Waals forces are, therefore, accounted for in NEMS where interactions occur at the atomic scale [115–120].

The effect of van der Waals forces on the pull-in voltage characteristics is studied in [115, 116], and in [117], approximate analytical expressions for the pull-in parameters are derived. Stiction in MEMSs due to van der Waals forces has been studied in [118], and in [119], the effect on the pull-in parameters of cantilever NEM switches is investigated.

In [120] the combined effect of the Casimir and the van der Waals forces on the instability of torsional NEM actuators has been investigated.

5. Summary

Table 1 summarizes the electromechanical models for the electrostatically actuated MEMSs discussed above, and groups investigators according to some of the main modeling features and solution techniques.

In any review paper it is inevitable that some very important and fundamental works have been overlooked. Please accept our apologies if we have failed to notice your work.

References

[1] Fargas Marquès A, Costa Castelló R and Shkel A M 2005 Modelling the electrostatic actuation of MEMS: state of the art 2005 *Technical Report*

[2] Burns D, Zook J, Horning R, Herb W and Guckel H 1995 Sealed-cavity resonant microbeam pressure sensor *Sensors Actuators* A **48** 179–86

[3] Judy J K 2001 Microelectromechanical systems (MEMS): fabrication, design and applications *Smart Mater. Struct.* **10** 1115–34

[4] Pelesko J A and Bernstein D H 2002 *Modeling MEMS and NEMS* (London: Chapman and Hall) chapter 7

[5] Newell W 1968 Miniaturization of tuning forks *Science* **161** 1320–6

[6] Nguyen C T C, Katehi L P B and Rebeiz G M 1998 Micromachined devices for wireless communications *Proc. IEEE* **86** 1756–68

[7] Juneau T, Unterkofler K, Seliverstov T, Zhang S and Judy M 2003 Dual-axis optical mirror positioning using a nonlinear closed-loop controller *TRANSDUCERS, 12th Int. Conf. on Solid-State Sensors, Actuators and Microsystems* vol 1, pp 560–3

[8] Hung E S and Senturia S D 1999 Extending the travel range of analog-tuned electrostatic actuators *J. Microelectromech. Syst.* **8** 497–505

[9] Gupta R K and Senturia S D 1997 Pull-in time dynamics as a measure of absolute pressure *MEMS'97: Proc. IEEE Int. Workshop on Microelectromechanical Systems (Nagoya, Jan. 1997)* pp 290–4

[10] Teymoori M M and Abbaspour-Sani E 2002 A novel electrostatic micromachined pump for drug delivery systems *IEEE Int. Conf. on Semiconductor Electronics, Proc. ICSE 2002* pp 105–9

[11] Chu P B, Nelson P R, Tachiki M L and Pister K S 1996 Dynamics of polysilicon parallel-plate electrostatic actuators *Sensors Actuators* A **52** 216–20

[12] Abdel-Rahman E M, Younis M I and Nayfeh A H 2002 Characterization of the mechanical behavior of an electrically actuated microbeam *J. Micromech. Microeng.* **12** 759–66

[13] Nayfeh A H and Younis M I 2005 Dynamics of MEMS resonators under superharmonic and subharmonic excitations *J. Micromech. Microeng.* **15** 1840–7

[14] Rhoads J F, Shaw S W and Turner K L 2006 The nonlinear response of resonant microbeam systems with purely-parametric electrostatic actuation *J. Micromech. Microeng.* **16** 890–9

[15] Tilmans H A and Legtenberg R 1994 Electrostatically driven vacuum-encapsulated polysilicon resonators: part II. Theory and performance *Sensors Actuators* A **45** 67–84

[16] Younis M I and Nayfeh A H 2003 A study of the nonlinear response of a resonant microbeam to an electric actuation *Nonlinear Dyn.* **31** 91–117

[17] Krylov S and Maimon R 2004 Pull-in dynamics of an elastic beam actuated by continuously distributed electrostatic force *J. Vib. Acoust.* **126** 332–42

[18] Kuang J-H and Chen C-J 2004 Dynamic characteristics of shaped micro-actuators solved using the differential quadrature method *J. Micromech. Microeng.* **14** 647–55

[19] Xie W C, Lee H P and Lim S P 2003 Nonlinear dynamic analysis of MEMS switches by nonlinear modal analysis *Nonlinear Dyn.* **31** 243–56

[20] Taylor G I 1968 The coalescence of closely spaced drops when they are at different electric potentials *Proc. R. Soc.* A **306** 423–34

[21] Nathanson H C, Newell W E, Wickstrom R A and Davis J R 1967 The resonant gate transistor *IEEE Trans. Electron Devices* **14** 117–33

[22] Tilmans H A and Legtenberg R 1994 Electrostatically driven vacuum-encapsulated polysilicon resonators: part I. Design and fabrication *Sensors Actuators* A **45** 57–66

[23] Pamidighantam S, Puers R, Baert K and Tilmans H A C 2002 Pull-in voltage analysis of electrostatically actuated beam structures with fixed–fixed and fixed-free end conditions *J. Micromech. Microeng.* **12** 458–64

[24] Castañer L M and Senturia S D 1999 Speed-energy optimization of electrostatic actuators based on pull-in *J. Microelectromech. Syst.* **8** 290–8

[25] Li G and Aluru N R 2003 Efficient mixed-domain analysis of electrostatic MEMS *IEEE Trans. Comput.-Aided Des. Integr. Circuits Syst.* **22** 1228–42

[26] Batra R C 2005 *Elements of Continuum Mechanics* (Reston, VA: American Institute of Aeronautics and Astronautics)

[27] Michopoulos J G, Farhat C and Fish J 2005 Modeling and simulation of multiphysics systems *Trans. ASME* **5** 198–213

[28] Pelesko J and Triolo A 2001 Nonlocal problems in MEMS device control *J. Eng. Math.* **41** 345–66

[29] Shi F, Ramesh P and Mukherjee S 1995 On the application of 2D potential theory to electrostatic simulation *Commun. Numer. Methods Eng.* **11** 691–701

[30] Schlichting H 1979 *Boundary-Layer Theory* (New York: McGraw-Hill)

[31] Microcosm Technologies http://www.memcad.com/

[32] Senturia S D, Harris R M, Johnson B P, Kim S, Nabors K, Shulman M A and White J K 1992 A computer-aided design system for microelectromechanical systems (MEMCAD) *J. Microelectromech. Syst.* **1** 3–13

[33] Coventor Inc. www.coventor.com

[34] Shi F, Ramesh P and Mukherjee S 1996 Dynamic analysis of microelectromechanical systems *Int. J. Numer. Methods Eng.* **39** 4119–39

[35] Gabbay L D, Mehner J E and Senturia S D 2000 Computer-aided generation of nonlinear reduced-order dynamic macromodels II: non-stress-stiffened case *J. Microelectromech. Syst.* **9** 262–9

[36] Aluru N R 1999 A reproducing kernel particle method for meshless analysis of microelectromechanical systems *Comput. Mech.* **23** 324–38

[37] Shrivastava V, Aluru N R and Mukherjee S 2004 Numerical analysis of 3D electrostatics of deformable conductors using a Lagrangian approach *Eng. Anal. Bound. Elem.* **28** 583–91

[38] Li G and Aluru N R 2002 A Lagrangian approach for electrostatic analysis of deformable conductors *J. Microelectromech. Syst.* **11** 245–54

[39] De S K and Aluru N R 2004 Full-Lagrangian schemes for dynamic analysis of electrostatic MEMS *J. Microelectromech. Syst.* **13** 737–58

[40] De S K and Aluru N R 2006 Coupling of hierarchical fluid models with electrostatic and mechanical models for the dynamic analysis of MEMS *J. Micromech. Microeng.* **16** 1705–19

[41] Bochobza-Degani O, Elata D and Nemirovsky Y 2002 An efficient DIPIE algorithm for CAD of electrostatically actuated MEMS devices *J. Microelectromech. Syst.* **11** 612–20

[42] Senturia S D, Aluru N R and White J 1997 Simulating the behavior of MEMS devices: computational methods and needs *IEEE Comput. Sci. Eng.* **4** 30–43

[43] O'Mahony C, Hill M, Duane R and Mathewson A 2003 Analysis of electromechanical boundary effects on the pull-in of micromachined fixed–fixed beams *J. Micromech. Microeng.* **13** S75–80

[44] Lishchynska M, Cordero N, Slattery O and O'Mahony C 2005 Modelling electrostatic behaviour of microcantilevers incorporating residual stress gradient and non-ideal anchors *J. Micromech. Microeng.* **15** S10–4

[45] Antman S S 2004 *Nonlinear Problems of Elasticity* (*Applied Mathematical Sciences*) 2nd edn (New York: Springer)

[46] Naghdi P M 1972 *The Theory of Shells and Plates* (*Handbuch der Physik* vol VIa/2) (Berlin: Springer) pp 425–640

[47] Naghdi P M 1980 Finite deformations of rods and shells *Proc. IUTAM Symp. on Finite Elasticity (The Hague/Boston/London, Aug. 1980)* ed D E Carlson and R T Shield, (Dordrecht: Martinus Nijhoff) pp 47–103

[48] Batra R C and Vidoli S 2002 Higher order piezoelectric plate theory derived from a three-dimensional variational principle *AIAA J.* **40** 91–104

[49] Vidoli S and Batra R C 2000 Derivation of plate and rod equations for a piezoelectric body from a mixed three-dimensional variational principle *J. Elast.* **59** 23–50

[50] Batra R C, Vidoli S and Vestroni F 2002 Plane waves and modal analysis in higher-order shear and normal deformable plate theories *J. Sound Vib.* **257** 63–88

[51] Timoshenko S 1970 *Theory of Elasticity* 3rd edn (New York: McGraw-Hill)

[52] Mansfield E H 1989 *The Bending & Stretching of Plates* 2nd edn (Cambridge: Cambridge University Press) chapter 9

[53] Palmer H B 1937 Capacitance of a parallel-plate capacitor by the Schwartz–Christoffel transformation *Trans. Am. Inst. Electr. Eng.* **56** 363–6

[54] Meijs N V D and Fokkema J T 1984 VLSI circuit reconstruction from mask topology *Integration* **2** 85–119

[55] Nishiyama H and Nakamura M 1990 Capacitance of a strip capacitor *IEEE Trans. Compon. Hybrids Manuf. Technol.* **13** 417–23

[56] Batra R C, Porfiri M and Spinello D 2006 Capacitance estimate for electrostatically actuated narrow microbeams *Micro Nano Lett.* **1** 71–3

[57] Pelesko J A and Driscoll T A 2005 The effect of the small-aspect-ratio approximation on canonical electrostatic MEMS models *J. Eng. Math.* **53** 239–52

[58] Krylov S and Seretensky S 2006 Higher order correction of electrostatic pressure and its influence on the pull-in behavior of microstructures *J. Micromech. Microeng.* **16** 1382–96

[59] Hamrock B J 2004 *Fundamentals of Fluid Film Lubrication* 2nd edn (New York: Dekker)

[60] Nayfeh A H and Younis M I 2004 A new approach to the modeling and simulation of flexible microstructures under the effect of squeeze-film damping *J. Micromech. Microeng.* **14** 170–81

[61] Gallis M A and Torczynski J R 2004 An improved Reynolds-equation model for gas damping of microbeam motion *J. Microelectromech. Syst.* **13** 653–59

[62] Mohite S S, Kesar H i, Sonti V R and Pratap R 2005 Analytical solutions for the stiffness and damping coefficients of squeeze films in MEMS devices with perforated back plates *J. Micromech. Microeng.* **15** 2083–92

[63] Collenz A, De Bona F, Gugliotta A and Soma A 2004 Large deflections of microbeams under electrostatic loads *J. Micromech. Microeng.* **14** 365–73

[64] Hamad E and Omar A 2006 An improved two-dimensional coupled electrostatic–mechanical model for RF MEMS switches *J. Micromech. Microeng.* **16** 1424–9

[65] Osterberg P M and Senturia S D 1997 M-TEST: a test chip for MEMS material property measurement using electrostatically actuated test structures *J. Microelectromech. Syst.* **6** 107–18

[66] Yang F 2002 Electromechanical instability of microscale structures *J. Appl. Phys.* **92** 2789–94

[67] Younis M I, Abdel-Rahman E M and Nayfeh A H 2003 A reduced-order model for electrically actuated microbeam-based MEMS *J. Microelectromech. Syst.* **12** 672–80

[68] Choi B and Lovell E G 1997 Improved analysis of microbeams under mechanical and electrostatic loads *J. Micromech. Microeng.* **7** 24–9

[69] Nayfeh A H, Younis M I and Abdel-Rahman E M 2005 Reduced-order models for MEMS applications *Nonlinear Dyn.* **41** 211–36

[70] Gorthi S, Mohanty A and Chatterjee A 2006 Cantilever beam electrostatic MEMS actuators beyond pull-in *J. Micromech. Microeng.* **16** 1800–10

[71] Abdel-Rahman E M and Nayfeh A H 2003 Secondary resonances of electrically actuated resonant microsensors *J. Micromech. Microeng.* **13** 491–501

[72] Liu Y, Liew K M, Hon Y C and Zhang X 2005 Numerical simulation and analysis of an electroactuated beam using a radial basis function *Smart Mater. Struct.* **14** 1163–71

[73] Nayfeh A H and Younis M I 2005 Dynamics of MEMS resonators under superharmonic and subharmonic excitations *J. Micromech. Microeng.* **15** 1840–7

[74] Brusa E and Munteanu M G 2006 Coupled-field FEM nonlinear dynamics analysis of continuous microsystems by non-incremental approach *Analog Integr. Circuits Signal Process.* **48** 7–14

[75] Rinaldi G, Packirisamy M and Stiharu I 2007 Dynamic testing of micromechanical structures under thermo-electro-mechanical influences *Measurement* **40** 563–74

[76] Rhoads J F, Shaw S W and Turner K L 2006 The nonlinear response of resonant microbeam systems with purely-parametric electrostatic actuation *J. Micromech. Microeng.* **16** 890–9

[77] Najar F, Choura S, El-Borgi S, Abdel-Rahman E M and Nayfeh A H 2006 Modeling and design of variable-geometry electrostatic microactuators *J. Micromech. Microeng.* **16** 2449–57

[78] Batra R C, Porfiri M and Spinello D 2006 Electromechanical model of electrically actuated narrow microbeams *J. Microelectromech. Syst.* **15** 1175–89

[79] Andreaus U, Batra R C and Porfiri M 2005 Vibrations of cracked Euler–Bernoulli beams using meshless local Petrov–Galerkin (MLPG) method *CMES: Comput. Model. Eng. Sci.* **9** 111–32

[80] Atluri S N and Shen S 2002 The meshless local Petrov–Galerkin (MLPG) method: a simple and less-costly alternative to the finite element and boundary element methods *CMES: Comput. Model. Eng. Sci.* **3** 11–51

[81] Atluri S N, Cho J Y and Kim H-G 1999 Analysis of thin beams, using the meshless local Petrov–Galerkin method, with generalized moving least squares interpolations *Comput. Mech.* **24** 334–47

[82] Batra R C, Porfiri M and Spinello D 2007 Vibrations of narrow microbeams predeformed by an electric field *J. Sound Vib.* available online (doi:10.1016/j.jsv.2007.07.030)

[83] Hung E S and Senturia S D 1999 Generating efficient dynamical models for microelectromechanical systems from a few finite-element simulation runs *J. Microelectromech. Syst.* **8** 280–9

[84] Liang Y C, Lin W Z, Lee H P, Lim S P, Lee K H and Feng D P 2001 A neural-network-based method of model reduction for the dynamic simulation of MEMS *J. Micromech. Microeng.* **11** 226–33

[85] Yang Y-J, Cheng S-Y and Shen K-Y 2004 Macromodeling of coupled-domain MEMS devices with electrostatic and electrothermal effects *J. Micromech. Microeng.* **14** 1190–6

[86] Zhang C, Xu G and Jiang Q 2004 Characterization of the squeeze film damping effect on the quality factor of a microbeam resonator *J. Micromech. Microeng.* **14** 1302–6

[87] Mukherjee S, Bao Z, Roman M and Aubry N 2005 Nonlinear mechanics of MEMS plates with a total Lagrangian approach *Comput. Struct.* **83** 758–68

[88] Telukunta S and Mukherjee S 2006 Fully Lagrangian modeling of MEMS with thin plates *J. Microelectromech. Syst.* **15** 795–810

[89] Ng T Y, Jiang T Y, Lam K Y and Reddy J N 2004 A coupled field study on the non-linear dynamic characteristics of an electrostatic micropump *J. Sound Vib.* **273** 989–1006

[90] Chao P C-P, Chiu C-W and Tsai C-Y 2006 A novel method to predict the pull-in voltage in a closed form for micro-plates actuated by a distributed electrostatic force *J. Micromech. Microeng.* **16** 986–98

[91] Nayfeh A H and Younis M I 2004 Modeling and simulations of thermoelastic damping in microplates *J. Micromech. Microeng.* **14** 1711–7

[92] Machauf A, Nemirovsky Y and Dinnar U 2005 A membrane micropump electrostatically actuated across the working fluid *J. Micromech. Microeng.* **15** 2309–16

[93] Zhao X, Abdel-Rahman E M and Nayfeh A H 2004 A reduced-order model for electrically actuated microplates *J. Micromech. Microeng.* **14** 900–6

[94] Vogl G W and Nayfeh A H 2005 A reduced-order model for electrically actuated clamped circular plates *J. Micromech. Microeng.* **15** 684–90

[95] Pelesko J A 2002 Mathematical modeling of electrostatics MEMS with tailored dielectric properties *SIAM J. Appl. Math.* **62** 888–908

[96] Pelesko J A and Chen X Y 2003 Electrostatic deflections of circular elastic membranes *J. Electrostat.* **57** 1–12

[97] Batra R C, Porfiri M and Spinello D 2006 Analysis of electrostatic MEMS using meshless local Petrov–Galerkin (MLPG) method *Eng. Anal. Bound. Elem.* **30** 949–62

[98] Doedel E, Keller H B and Kernevez J P 1991 Numerical analysis and control of bifurcation problems (I) Bifurcation in finite dimensions *Int. J. Bifurcation Chaos* **1** 493–520

[99] Lamoreaux S K 2005 The Casimir force: background, experiments, and applications *Rep. Prog. Phys.* **68** 201–36

[100] Borgag M, Mohideen U and Mostepanenko V M 2001 New developments in the Casimir effect *Phys. Rep.* **353** 1–205

[101] Casimir H B G 1948 On the attraction between two perfectly conducting plates *Proc. K. Ned. Akad. Wet.* **51** 793

[102] Borgag M 2006 Casimir effect for a sphere and a cylinder in front of a plane and corrections to the proximity force theorem *Phys. Rev.* D **73** 125018

[103] Gies H and Klingmüller K 2006 Casimir effect for curved geometries: proximity-force-approximation validity limits *Phys. Rev. Lett.* **96** 220401

[104] Michael Serry F, Walliser D and Jordan Maclay G 1998 The role of the Casimir effect in the static deflection and stiction of membrane strips in microelectromechanical systems (MEMS) *J. Appl. Phys.* **84** 2501–6

[105] Ding J-N, Wen S-Z and Meng Y-G 2001 Theoretical study of the sticking of a membrane strip in MEMS under the Casimir effect *J. Micromech. Microeng.* **11** 202–8

[106] Bárcenas J, Reyes L and Esquivel-Sirvent R 2005 Scaling of micro- and nanodevices actuated by Casimir forces *Appl. Phys. Lett.* **87** 263106

[107] Buks E and Roukes M L 2001 Stiction, adhesion energy, and the Casimir effect in micromechanical systems *Phys. Rev.* B **63** 033402

[108] Buks E and Roukes M L 2001 Metastability and the Casimir effect in micromechanical systems *Europhys. Lett.* **54** 220

[109] Lin W-H and Zhao Y-P 2005 Casimir effect on the pull-in parameters of nanometer switches *Microsyst. Technol.* **11** 80–5

[110] Wang C, Guo W and Feng Q 2005 Deflection and stability of membrane structures under electrostatic and Casimir forces in microelectromechanical systems *Acta Mech.* **180** 49–60

[111] Batra R C, Porfiri M and Spinello D 2007 Effects of Casimir force on pull-in instability in micromembranes *Europhys. Lett.* **77** 20010

[112] Batra R C, Porfiri M and Spinello D 2007 Reduced-order models for microelectromechanical rectangular and circular plates incorporating the Casimir force *Int. J. Solid Struct.* submitted

[113] Batra R C, Porfiri M and Spinello D 2007 Vibrations and pull-in instabilities of microelectromechanical von Karman elliptic plates incorporating the Casimir force *J. Sound Vibration* submitted

[114] Lifshitz E M 1956 The theory of molecular attractive forces between solids *Sov. Phys.—JETP* **2** 73–83

[115] Dequesnes M, Rotkin S V and Aluru N R 2002 Calculation of pull-in voltages for carbon-nanotube-based nanoelectromechanical switches *Nanotechnology* **13** 120–31

[116] Dequesnes M, Tang Z and Aluru N R 2004 Static and dynamic analysis of carbon nanotube-based switches *Trans. ASME, J. Eng. Mater. Technol.* **126** 230–7

[117] Rotkin S V 2002 Analytical calculations for nanoscale electromechanical systems *Electrochem. Soc. Proc.* **6** 90–7

[118] van Spengen W M, Puers R and De Wolf I 2002 A physical model to predict stiction in MEMS *J. Micromech. Microeng.* **12** 702–13

[119] Ramezani A, Alasty A and Akbari J 2006 Influence of van der Waals force on the pull-in parameters of cantilever type nanoscale electrostatic actuators *Microsyst. Technol.* **12** 1153–61

[120] Guo J-G and Zhao Y-P 2004 Influence of van der Waals and Casimir forces on electrostatic torsional actuators *J. Microelectromech. Syst.* **13** 1027–35